Collectivity in Pb-196,Pb-198 isotopes probed in Coulomb-excitation experiments at REX-ISOLDE

Pakarinen, J.

2017-06

Pakarinen , J , Grahn , T , Gaffney , L P , Algora , A , Bauer , C , Blazhev , A , Bree , N , Cocolios , T E , De Witte , H , Diriken , J , Fernier , P , K , H-K K , Herzan , A , Huyse , M , Iwanicki , J , Jakobsson , U , Jenkins , D , Kesteloot , N , Konki , J , Lannoo , B , Papadakis , P , Peura , P , Rahkila , P , Rainovski , G , Rapisarda , E , Reiter , P , Sambi , S , Scheck , M , Seibeck , B , Seidlitz , M , Stora , T , Van Duppen , P , Warr , N , Wenander , F , Vermeulen , M J , Voulot , D , Wrzosek-Lipska , K & Zielinska , M 2017 , ' Collectivity in Pb-196,Pb-198 isotopes probed in Coulomb-excitation experiments at REX-ISOLDE ' , Journal of Physics G: Nuclear and Particle Physics , vol. 44 , no. 6 , 064009 . https://doi.org/10.1088/1361-6471/aa6753

http://hdl.handle.net/10138/231711
https://doi.org/10.1088/1361-6471/aa6753

Collectivity in ^{196,198}Pb isotopes probed in Coulomb-excitation experiments at REX-ISOLDE

OPEN ACCESS
IOP Publishing

Made open access 12 September 2017
Journal of Physics G: Nuclear and Particle Physics

J. Phys. G: Nucl. Part. Phys. **44** (2017) 064009 (10pp) https://doi.org/10.1088/1361-6471/aa6753

Collectivity in ^{196,198}Pb isotopes probed in Coulomb-excitation experiments at REX-ISOLDE

J Pakarinen[1,2,3], T Grahn[1,3], L P Gaffney[4,5], A Algora[6,7], C Bauer[8], A Blazhev[9], N Bree[4], T E Cocolios[2], H De Witte[4], J Diriken[4], P Fernier[2], K Hadyńska-Klęk[10], A Herzáň[1], M Huyse[4], J Iwanicki[10], U Jakobsson[1,3], D Jenkins[11], N Kesteloot[4,12], J Konki[1,3], B Lannoo[4], P Papadakis[5], P Peura[1,3], P Rahkila[1,3], G Rainovski[13], E Rapisarda[4], P Reiter[8], S Sambi[4], M Scheck[5], B Seibeck[8], M Seidlitz[8], T Stora[2], P Van Duppen[4], N Warr[8], F Wenander[2], M J Vermeulen[11], D Voulot[2], K Wrzosek-Lipska[10] and M Zielińska[14]

[1] University of Jyvaskyla, Department of Physics, P O Box 35, FI-40014 University of Jyvaskyla, Finland
[2] ISOLDE, CERN, CH-1211, Geneva, Switzerland
[3] Helsinki Institute of Physics, FI-00014, Helsinki, Finland
[4] Instituut voor Kern- en Stralingsfysica, K. U. Leuven, B-3001 Leuven, Belgium
[5] Oliver Lodge Laboratory, University of Liverpool, Liverpool, L69 7ZE, United Kingdom
[6] Instituto de Fisica Corpuscular, CSIC-Univ. Valencia, E-46071 Valencia, Spain
[7] Institute of Nuclear Research of the Hungarian Academy of Sciences, Debrecen, H-4026, Hungary
[8] Institut für Kernphysik, TU Darmstadt, D-64289 Darmstadt, Germany
[9] Institut für Kernphysik, Universität zu Köln, D-50937 Köln, Germany
[10] Heavy Ion Laboratory, Warsaw University, PL-02-093 Warsaw, Poland
[11] Department of Physics, University of York, YO10 5DD, United Kingdom
[12] Studiecentrum voor Kernenergie/Centre de l'Energie Nucléaire (SCK•CEN), B-2400 Mol, Belgium
[13] Faculty of Physics, St. Kliment Ohridski University of Sofia, 1164 Sofia, Bulgaria
[14] IRFU/SPhN, CEA Saclay, F-91191 Gif-sur-Yvette, France

E-mail: janne.pakarinen@jyu.fi

Received 31 October 2016, revised 16 March 2017
Accepted for publication 17 March 2017
Published 3 May 2017

Abstract

The neutron-deficient ^{196,198}Pb isotopes have been studied in Coulomb-excitation experiments employing the Miniball γ-ray spectrometer and radioactive

ion beams from the REX-ISOLDE post-accelerator at CERN. The reduced transition probabilities of the first excited 2^+ states in ^{196}Pb and ^{198}Pb nuclei have been measured for the first time. Values of $B(E2) = 18.2^{+4.8}_{-4.1}$ W.u. and $B(E2) = 13.1^{+4.9}_{-3.5}$ W.u., were obtained, respectively. The experiment sheds light on the development of collectivity when moving from the regime governed by the generalised seniority scheme to a region, where intruding structures, associated with different deformed shapes, start to come down in energy and approach the spherical ground state.

Keywords: Coulomb excitation, radioactive ion beams, gamma-ray spectroscopy, γ transitions and level energies

(Some figures may appear in colour only in the online journal)

1. Introduction

Atomic nuclei can be considered as unique laboratories for studies of exotic phenomena. The movements of single neutrons or protons and their tendency to couple, combined with collective motions of groups of nucleons, can result in different intrinsic configurations at degenerate energies. These different configurations can present different shapes, giving rise to a phenomenon known as the shape coexistence [1]. A few prominent regions in the chart of nuclei can be found where the shape coexistence is inherent [2]. In particular, one of the most explored regions can be found around the neutron-deficient ^{186}Pb nucleus (see [1] and references therein). In that region, the competing deformed structures, associated with proton multiparticle-multihole excitations across the $Z = 82$ shell closure, intrude down to the energies close to the spherical ground state [3–9]. The main support for this picture comes from the hindrance factors obtained in α-decay fine-structure measurements [10]. Calculations using the deformed mean-field approach, essentially equivalent to the shell-model method, associate intruder configurations with prolate and oblate shape [11–15]. Together with the spherical ground state, they result in a unique triplet of shape-coexisting 0^+ states in $^{186}Pb_{104}$ [3]. The low-lying 0^+ states form the basis for the rotational bands observed in the even-mass Pb isotopes [16–21]. The level-energy systematics of Pb isotopes with $A \leqslant 204$ is shown in figure 1.

In order to map the boundaries where the generalised seniority regime changes to the region characterised by intruding configurations it is important to measure transition probabilities between the low-lying states [22, 23]. Lifetime measurements in the region of interest employing fusion–evaporation reactions are challenging due to the presence of the isomeric states preventing the prompt feeding of the low-lying states. On the other hand, these states have too short lifetimes to be measured in decay experiments. Coulomb excitation (Coulex) provides an alternative approach to direct lifetime measurements, and moreover is sensitive to quadrupole moments of excited states. However, with stable-ion beams the Coulex method can only be applied to stable or long-lived nuclei. For the Coulex of short-lived nuclei, these nuclei must be available as radioactive ion beams (RIB). Coulex of short-lived nuclei has recently been employed at the first generation RIB facilities and it is one of the most important methods for probing collectivity in exotic nuclei as the production cross sections are much higher than for example in fusion–evaporation reactions.

Today the selection of available RIBs has been successfully extended into very heavy nuclei such as Rn and Ra [24] in the leading RIB ISOL-facility REX-ISOLDE at CERN [25].

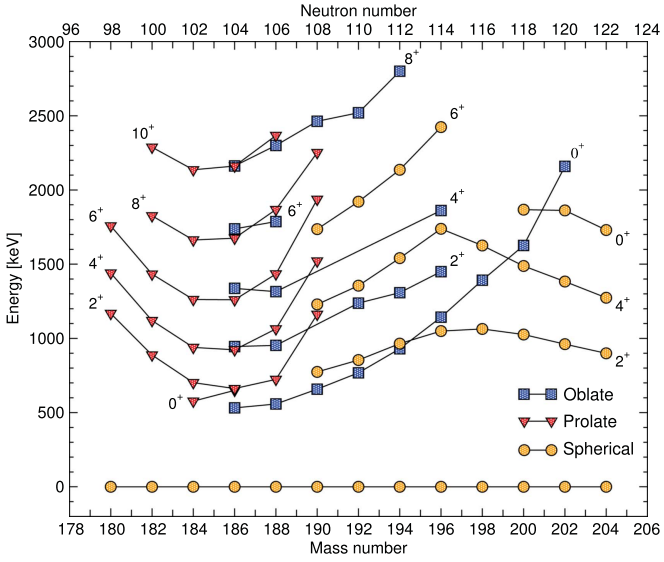

Figure 1. Level-energy systematics of the neutron-deficient Pb isotopes adapted from [8]. Levels associated with different intrinsic configurations are connected and labelled according to proposed shapes. Reproduced from [8]. © IOP Publishing Ltd. All rights reserved.

Relevant to this study, collectivity in this region has been studied in Coulex experiments in the even-mass $^{182-188}$Hg, $^{196-202}$Po and $^{202-206}$Rn isotopes [26–28] and in the lifetime measurements of even-mass $^{180-188}$Hg, ^{186,188}Pb and ^{194,196}Po nuclei [29–33]. The role of Coulex experiments will become increasingly important at HIE-ISOLDE and with the advent of next-generation RIB facilities.

2. Experimental technique

The experiment was performed at the REX-ISOLDE facility, CERN [25]. The nuclei of interest were produced by bombarding a high temperature UC_x target with 1.4 GeV proton beam provided by PS-Booster with intensity up to 2 μA. The RIB were extracted employing the RILIS laser ion source [34]. Subsequently, they were mass selected utilising the high resolution separator before being delivered to the REXTRAP Penning trap for cooling and bunching and REXEBIS electron-beam ion source for charge breeding. Finally, the REX-ISOLDE post-accelerator was employed to deliver the RIB of ^{196,198}Pb at 2.82 MeV/u to the Miniball γ-ray spectrometer [35]. Miniball is an array of eight triple-cluster Ge-detectors, where each crystal is six-fold segmented. At Miniball, the RIB impinged on a 2 mg cm^{-2} thick ^{112}Cd target. The beam energy was chosen to fulfil the safe energy criterion [36], in other words to ensure that all interactions in the scattering processes were purely electromagnetic. The beam intensity on the Miniball target varied between 2.5×10^5 and 5.0×10^5 pps. The scattered beam and target recoils were detected with the CD detector at 32.9 mm downstream from the target. The CD detector consists of four individual double-sided silicon strip detector quadrants. At the front side the quadrants are divided in 16 annular strips, while the pairwise coupling of the 24 backside strips results in 12 strips in radial direction. The γ rays following the de-excitation of the Coulomb-excited states

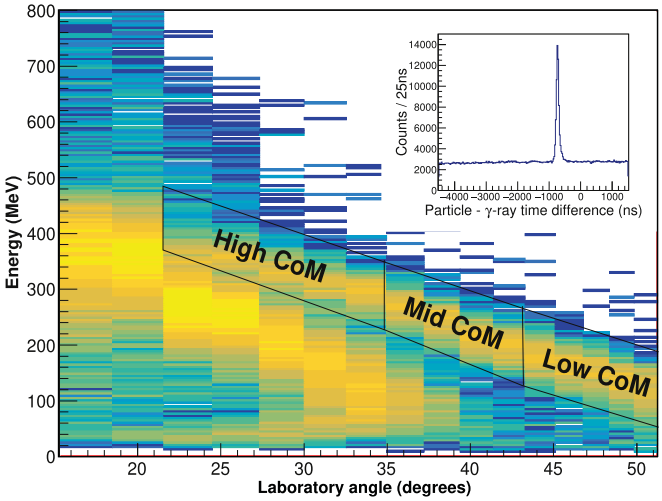

Figure 2. Particles measured in the CD detector in the ^{196}Pb experiment. The three different angular ranges selected in the analysis have been labelled. The corresponding particle-γ-ray time difference spectrum is shown in the inset.

were recorded with the Miniball Ge-detector array [35]. The relatively high granularity of Miniball (144 segments) and the CD detector (768 'pixels') allowed for kinematic correction to be made.

The Ge-detectors were equipped with digital electronics employing the DGF-4C Revision D modules from XIA [37], while signals from the CD detector were passed through conventional analogue electronics consisting of RAL109 shaping/discriminator amplifiers and MADC-32 peak sensing ADCs from Mesytec [38]. The detector signals were recorded in the buffer of electronics modules during the 800 μs beam-on time window, triggered by the release of particles from the REXEBIS for post-acceleration, and during the following 800 μs beam-off time window. Outside of the beam-on time window, no beam from REX-ISOLDE was impinging on the Miniball target, thus the beam-off time window was used to assess the amount of background radiation. The buffer was subsequently read-out to disk in between the beam-on/off windows. The MARABOU data acquisition system [39], based on the multi branch system (MBS) [40] and the ROOT framework [41], was used. The MBS took care of the data read-out, event building and data transport, while ROOT provided tools for run control, histogramming, data storage and the on- and off-line analysis of the data.

For detailed analysis of the Coulex data, the understanding of the beam composition is essential. While the Pb ions were produced via laser ionisation, the neighbouring Tl nuclei were surface ionised in the target ion source. These isobaric contaminants survived all the separation and beam manipulation stages and were post-accelerated along the Pb beams of interest. In order to correct for the target excitations arising from the Tl beam impinging on the Miniball target, the beam composition was assessed carefully [42]. The beam purity of 98.7 $\pm$ 0.5% and 98.6 $\pm$ 0.7% was extracted for ^{196}Pb and ^{198}Pb, respectively. Apart from the Tl isobaric impurities, no other contaminants were found in the radioactive ion beam.

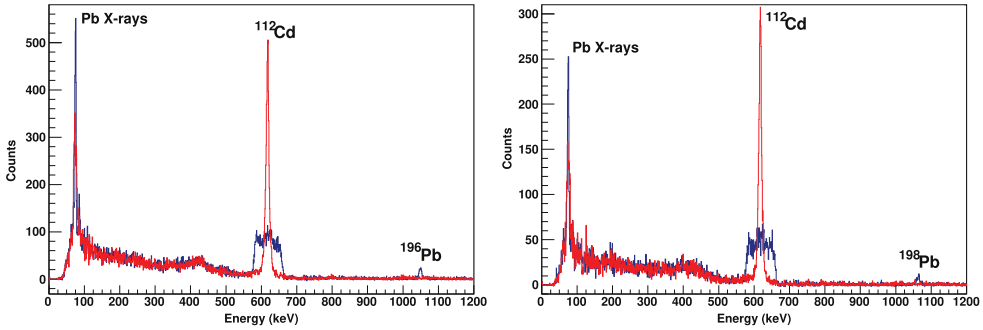

Figure 3. Particle-gated background-subtracted γ-ray energy spectra Doppler-corrected for the scattered beam (blue) and target (red) recoils obtained in the ^{196}Pb (left) and ^{198}Pb (right) experiments. Prominent peaks have been labelled.

Table 1. Angular ranges used in the analysis in laboratory (θ_{lab}) and centre of mass (θ_{CoM}) coordinate systems. Angles in both experiments (^{196}Pb and ^{198}Pb) are the same down to the last given decimal.

Gate as in figure 2	Scattered target (θ_{lab})	Scattered beam (θ_{CoM})	Scattered target (θ_{CoM})
High CoM	21.6°–34.9°	43.3°–69.9°	136.7°–110.1°
Mid CoM	35.0°–43.3°	70.1°–86.6°	109.9°–93.4°
Low CoM	43.3°–51.2°	86.7°–102.5°	93.3°–77.5°

3. Analysis and results

The analysis is based on the data collected during the beam-on time window and the laser-ionisation ion source in operation. The laser on–off technique was employed to define the amount of target excitations originating from the beam impurities impinging on the target [42]. The experiment was performed in inverse kinematics and the scattered target recoils were always observed in coincidence with the scattered beam. This was exploited in the analysis by requesting two detected hits in the CD detector, which enabled more precise reconstruction of kinematics and therefore better Doppler correction for the energies of observed γ rays. Although the kinematic branches for the scattered beam and target recoils could not be distinguished for the two innermost strips, the statistics were sufficient to divide the CD detector in three different angular ranges in both ^{196}Pb and ^{198}Pb experiments. In figure 2, the particle energy with respect to the scattering angle is shown. The selected angular ranges for the scattered target recoils in the laboratory coordinates and the corresponding centre of mass angles for the scattered beam and target recoils are listed in table 1.

Prompt particle-γ-ray time condition (with a time gate width of 400 ns) was set to further purify the γ-ray energy spectra from the random γ rays in coincidence with the particles. An example of a particle-γ-ray time difference spectrum obtained in the ^{196}Pb experiment is shown in the inset of figure 2.

In figure 3, prompt particle-gated background-subtracted γ-ray energy spectra Doppler-corrected for the scattered beam and target recoils obtained in both ^{196}Pb and ^{198}Pb experiments are shown. When correcting for the scattered beam (blue curve), two prominent peaks can be found; one that can be associated with the Pb x-rays and the other with the $2_1^+ \rightarrow 0_1^+$

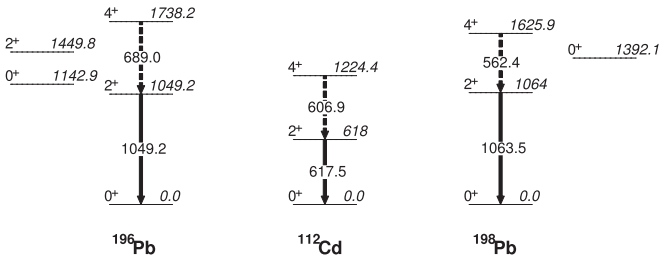

Figure 4. Partial level schemes of relevant nuclei in the present work. The observed γ rays are shown with solid arrows, while the transitions connecting to the buffer states [44] as declared in the GOSIA2 analysis are indicated with dashed arrows. Other known levels below the buffer states are shown for completeness.

Table 2. Results obtained in the present work including spectroscopic data for ^{112}Cd, which is taken from [45]. For the ^{196,198}Pb nuclei, values for transition matrix elements are translated to reduced transition probabilities ($B(E2)$ given both in eb and Weisskopf units (W.u.). Diagonal matrix elements are also translated to spectroscopic quadrupole moments $Q_{\rm sp}$.

	^{196}Pb	^{198}Pb	^{112}Cd
$\langle 0_1^+ \|\|\hat{M}(E2)\|\|2_1^+\rangle$ (eb)	$0.79^{+0.10}_{-0.09}$	$0.67^{+0.11}_{-0.10}$	0.697(20)
$B(E2: 0_1^+ \rightarrow 2_1^+)$ (e^2b^2)	$0.62^{+0.16}_{-0.14}$	$0.45^{+0.17}_{-0.12}$	
$B(E2: 2_1^+ \rightarrow 0_1^+)$ (W.u.)	$18.2^{+4.8}_{-4.1}$	$13.1^{+4.9}_{-3.5}$	
$\langle 2_1^+ \|\|\hat{M}(E2)\|\|2_1^+\rangle$ (eb)	$-1.0^{+0.9}_{-0.8}$	$0.5^{+1.3}_{-1.1}$	−0.488(150)
$Q_{\rm sp}$ (eb)	$-0.8^{+0.7}_{-0.6}$	$0.4^{+1.0}_{-0.9}$	
$\langle 2_1^+ \|\|\hat{M}(E2)\|\|4_1^+\rangle$ (eb)			1.342(70)

transition. The peak associated with the ^{112}Cd target excitation sharpens when Doppler correction is applied for the scattered target recoils, in that case the $2_1^+ \rightarrow 0_1^+$ transitions in ^{196,198}Pb nuclei are totally smeared out.

The relevant excited states in the target and beam nuclei for the present work are summarised in figure 4, where partial level schemes of ^{112}Cd, ^{196}Pb and ^{198}Pb are shown. As seen in figure 3, only the 2_1^+ states in the target and beam nuclei were populated. The $2_1^+ \rightarrow 4_1^+$ excitations shown as the dashed lines in figure 4 were not observed in the experiment. However, the 4_1^+ states were included in the GOSIA2 analysis as 'buffer states' in order to properly take into account possible two-step excitations, competing with the effect of the quadrupole moment of the 2_1^+ state on its excitation cross section. The matrix element data of ^{112}Cd used in the analysis are given in table 2.

In the present work, the cross sections measured for ^{196}Pb and ^{198}Pb were normalised for the observed target excitation. Therefore, the least-square fit code GOSIA2, which is adapted to such cases, was used for analysis [43, 44]. The power of GOSIA2 code is that it can simultaneously treat both target and beam excitations measured in a single experiment. This allows for analysis when very limited amount of experimental data is available (e.g. no existing lifetime data like in the present work) or when normalisation is not possible through Rutherford scattering yields. In the present work, the known $2_1^+ \rightarrow 0_1^+$ transition in ^{112}Cd was used for normalisation. In the least-square χ^2 fitting procedure, the two-dimensional surface consisting of transitional ($\langle 2_1^+ \|\|\hat{M}(E2)\|\|0_1^+\rangle$) and diagonal matrix elements ($\langle 2_1^+ \|\|\hat{M}(E2)\|\|2_1^+\rangle$)

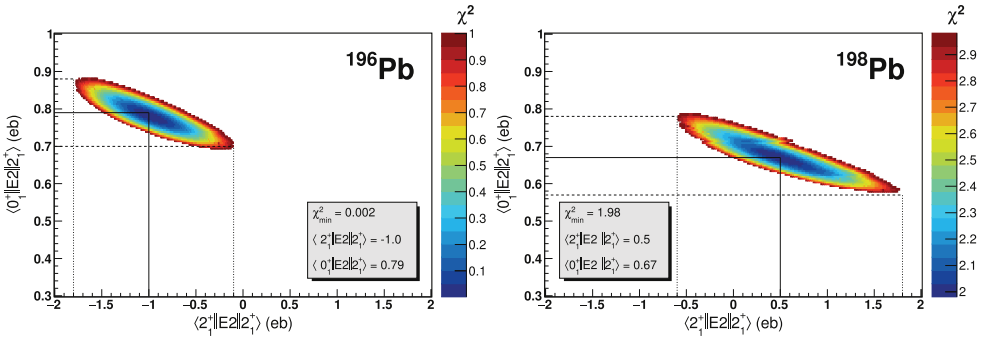

Figure 5. Two-dimensional χ^2 surfaces with respect to transitional and diagonal matrix elements for ^{196}Pb and ^{198}Pb obtained in the present work. 1σ cuts are applied with the condition that $\chi^2 \leqslant \chi^2_{\rm min} + 1$. Projections and locations of $\chi^2_{\rm min}$ on axis are drawn.

was scanned to search for the best solution at $\chi^2_{\rm min}$. The associated 1σ uncertainties were extracted by cutting the surface at $\chi^2 \leqslant \chi^2_{\rm min} + 1$ and projecting the cut to the relevant axis. The χ^2 surfaces and positions of $\chi^2_{\rm min}$ with cuts on $\chi^2_{\rm min} + 1$ obtained from the GOSIA2 analysis for ^{196}Pb and ^{198}Pb are plotted in figure 5. Full results together with spectroscopic data for ^{112}Cd used in the GOSIA2 analysis are given in table 2. The analysis technique is described in more details in [46].

4. Discussion

Very limited information on transition probabilities exists throughout the known Pb isotopic chain. The $B(E2; 0_1^+ \rightarrow 2_1^+)$ values in even-mass Pb isotopes close to the doubly-magic ^{208}Pb have been studied in inelastic scattering experiments employing variety of beams. An α-particle scattering experiment was carried out on ^{208}Pb [47], while electron scattering was employed to probe the ^{206}Pb and ^{208}Pb isotopes [48]. In 1978, Joye *et al* measured also the quadrupole moments in the ^{204}Pb and ^{206}Pb isotopes by using beams of ^{4}He, ^{12}C and ^{16}O nuclei in Coulex experiments [49]. The heaviest ^{210}Pb isotope with known $B(E2; 0_1^+ \rightarrow 2_1^+)$ value was studied in inelastic tritium and proton scattering from the radioactive ^{210}Pb target [50]. A couple of decades and lots of development work was required before the $B(E2; 0_1^+ \rightarrow 2_1^+)$ values in other Pb isotopes could be experimentally determined. In 2006, the recoil-distance Doppler shift technique was used to measure the lifetimes of the low-lying yrast states in ^{186}Pb and ^{188}Pb [32]. In addition to measurements reported in the present work, Coulex data have been obtained for the even-mass $^{188-194}$Pb isotopes [42] at ISOLDE.

In contrast to the lack of experimental data, several different theoretical calculations have predicted the transition probabilities of the first excited 2^+ states in the Pb isotopes. The low-lying collective excitations have been studied by performing a configuration mixing of angular momentum and particle-number projected self-consistent mean-field states employing the Skyrme (Sly6) interaction [14, 15, 19, 51]. This model qualitatively reproduced the variation of the spectra with neutron number and supported the picture of three different shapes lying close to the ground state near the $N = 104$ midshell. The interacting boson model (IBM) approximation calculations with configuration mixing for the even-mass $^{188-196}$Pb isotopes have been carried out [19, 52]. An iterative method based on the quasi-particle random-phase approximation (QRPA) has been developed and employed for the

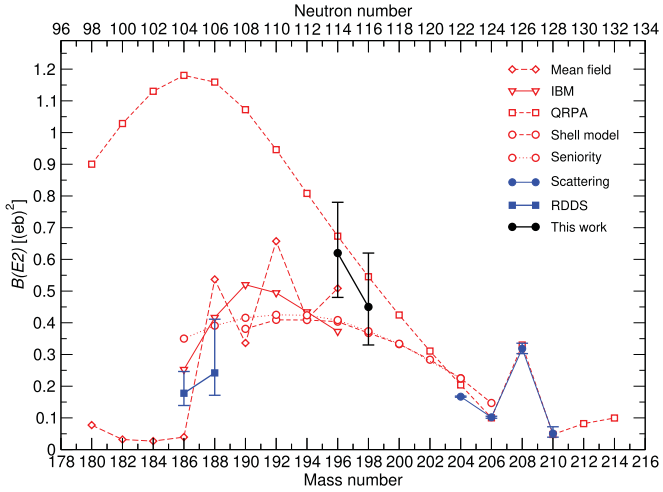

Figure 6. Reduced transition probabilities of the 2_1^+ states in the Pb isotopes. Values obtained by different theoretical approaches (open symbols) are connected with red dashed line. Experimental results from scattering and lifetime measurements (filled symbols) with uncertainties are shown in solid blue lines. Results from the present work are shown with filled black circles.

calculation of the low-lying vibrational states in the spherical minimum [54] and very recently, large-scale shell-model calculations including a number of neutron-hole orbitals in the model space were performed [55].

The existing experimental and theoretical data for the $B(E2; 0_1^+ \rightarrow 2_1^+)$ values throughout the Pb isotopic chain are combined in figure 6 for comparison. The IBM and mean-field calculations have provided data also on the other low-lying states, but these are not plotted for clarity. The QRPA and shell-model descriptions reproduce the values around the ^{208}Pb nucleus. Close to the midshell, the low-lying states are strongly mixed [20, 29, 32, 53], which makes direct comparison between experimental and theoretical values difficult as the transition probabilities are very sensitive to the amount of mixing. The $B(E2; 0_1^+ \rightarrow 2_1^+)$ value extracted for ^{198}Pb in the present work falls in between the QRPA and shell-model calculations, which are both covered within the experimental uncertainties. In ^{196}Pb the measured $B(E2; 0_1^+ \rightarrow 2_1^+)$ value matches the mean-field and QRPA predictions, but is larger than the one extracted in shell-model calculations. The measured values increase slightly when moving to the more neutron-deficient nucleus ^{196}Pb. The trend is similar to that of the QRPA calculations, although the measured transition probabilities are a bit smaller. According to the QRPA calculations, the 2_1^+ states are associated with two-quasineutron excitations predominantly to the $i_{13/2}$ shell in ^{196}Pb and to the $i_{13/2}$ or $f_{5/2}$ shell in ^{198}Pb. This interpretation is also in-line with the IBM and mean-field calculations, which suggest that the proton multiparticle-multihole excitations (i.e. deformed structures) are highly non-yrast in ^{196,198}Pb [15, 52]. The spectroscopic quadrupole moments $Q_{\rm sp}$ extracted for the 2_1^+ states are close to zero supporting the assignment of these states with the spherical shape.

The overall trend of the experimental $B(E2; 0_1^+ \rightarrow 2_1^+)$ values around ^{208}Pb and in ^{196,198}Pb is in line of the usual pattern, where such values maximise towards the neutron midshell. This result can be derived for example from the generalised seniority scheme or from the QRPA calculations, as in figure 6. Such pattern is observed to some extent in the Sn isotopes ($Z = 50$) [22]. However, in the Pb isotopes this breaks down at around the midshell.

The theoretical models in figure 6 that incorporate configuration mixing can reproduce the observed trend of decreasing $B(E2; 0_1^+ \rightarrow 2_1^+)$ values at the neutron midshell. This, together with other complementary data, suggests that this effect is due to the shape coexistence and mixing at low spin. To verify this further, more data would be most welcome to fill in the gaps between $N = 106$ and $N = 114$ and to provide additional data on higher-lying excitations in the Pb nuclei.

5. Summary

The collectivity of the first excited 2^+ states in the neutron-deficient ^{196}Pb and ^{198}Pb nuclei have been measured in Coulex experiments employing RIB in inverse kinematics. Results have been compared with the latest theoretical models and the $B(E2; 0_1^+ \rightarrow 2_1^+)$ values obtained are consistent with values extracted using the QRPA in the spherical minimum and large-scale shell-model calculations in the model space including a number of neutron-hole orbitals. Accordingly, the 2^+ states in the neutron-deficient ^{196}Pb and ^{198}Pb are suggested to be composed of two-quasineutron excitations to the $i_{13/2}$ or $f_{5/2}$ shells. The nuclei studied in present work lie half way in between the the closed neutron $N = 126$ shell and the neutron midshell at $N = 104$. Coulex in inverse kinematics is one of the very few methods to obtain information on transition probabilities in these isotopes. In order to improve the precision of the obtained experimental values, more data are needed. This could either mean simply performing a similar Coulex experiment or carrying out a complementary lifetime measurement employing a plunger device currently being developed for the RIB at Miniball [56].

Acknowledgments

The staff members of the REX-ISOLDE facility are gratefully acknowledged for providing smooth running conditions. This research project has been supported by a Marie Curie Intra-European Fellowship (contract number PIEF-GA-2008-219175) and by a Marie Curie Career Integration Grant (contract number 304033) of the European Community's 7th Framework Programme and by the Academy of Finland (contract numbers 265023 and 131665). In addition, the German BMBF under contracts 05P12PKFNE and 05P15PKCIA and 'Verbundprojekt 05P2015' and the Spanish MINECO FPA2011-24553 and FPA2014-52823-C2-1 projects are acknowledged.

References

[1] Heyde K and Wood J L 2011 *Rev. Mod. Phys.* **83** 1467
[2] Möller P, Sierk A J, Bengtsson R, Sagawa H and Ichikawa T 2009 *Phys. Rev. Lett.* **103** 212501
[3] Andreyev A N *et al* 2000 *Nature* **405** 430
[4] Van Duppen P, Coenen E, Deneffe K, Huyse M, Heyde K and Van Isacker P 1984 *Phys. Rev. Lett.* **52** 1974
[5] Heyde K, Schietse J and De Coster C 1991 *Phys. Rev.* C **44** 2216
[6] De Coster C, Decroix B and Heyde K 2000 *Phys. Rev.* C **61** 067306
[7] Julin R, Helariutta K and Muikku M 2001 *J. Phys. G: Nucl. Part. Phys.* **27** R109
[8] Julin R, Grahn T, Pakarinen J and Rahkila P 2016 *J. Phys. G: Nucl. Part. Phys.* **43** 024004
[9] De Witte H *et al* 2007 *Phys. Rev. Lett.* **98** 112502
[10] Van Duppen P and Huyse M 2000 *Hyperfine Interact.* **129** 149
[11] May F R, Pashkevich V V and Frauendorf S 1977 *Phys. Lett.* B **68** 113
[12] Nazarewicz W 1993 *Phys. Lett.* B **305** 195
[13] Rodríguez-Guzmán R R, Egido J L and Robledo L M 2004 *Phys. Rev.* C **69** 054319

[14] Duguet T, Bender M, Bonche P and Heenen P-H 2003 *Phys. Lett.* B **559** 201
[15] Bender M, Bonche P, Duguet T and Heenen P-H 2004 *Phys. Rev.* C **69** 064303
[16] Rahkila P *et al* 2010 *Phys. Rev.* C **82** 011303(R)
[17] Jenkins D G *et al* 2000 *Phys. Rev.* C **62** 021302
[18] Cocks J F C *et al* 1998 *Eur. Phys. J.* A **3** 17
[19] Pakarinen J *et al* 2005 *Phys. Rev.* C **72** 011304(R)
[20] Dracoulis G D *et al* 2004 *Phys. Rev.* C **69** 054318
[21] Dracoulis G D, Byrne A P and Baxter A M 1998 *Phys. Lett.* B **432** 37
[22] Görgen A and Korten W 2016 *J. Phys. G: Nucl. Part. Phys.* **43** 024002
[23] Wrzosek-Lipska K and Gaffney L P 2016 *J. Phys. G: Nucl. Part. Phys.* **43** 024012
[24] Gaffney L P *et al* 2013 *Nature* **497** 199
[25] Kester O *et al* 2003 *Nucl. Instrum. Methods* B **204** 20
[26] Bree N *et al* 2014 *Phys. Rev. Lett.* **112** 162701
[27] Kesteloot N *et al* 2015 *Phys. Rev.* C **92** 054301
[28] Gaffney L P *et al* 2015 *Phys. Rev.* C **91** 064313
[29] Dewald A *et al* 2003 *Phys. Rev.* C **68** 034314
[30] Gaffney L P *et al* 2014 *Phys. Rev.* C **89** 024307
[31] Grahn T *et al* 2009 *Phys. Rev.* C **80** 014324
[32] Grahn T *et al* 2006 *Phys. Rev. Lett.* **97** 062501
[33] Grahn T *et al* 2009 *Phys. Rev.* C **80** 014323
[34] Fedoseyev V N, Huber G, Köster U, Lettry J, Mishin V I, Ravn H, Sebastian V and (the ISOLDE Collaboration) 2000 *Hyperfine Interact.* **127** 409
[35] Warr N *et al* 2013 *Eur. Phys. J.* A **49** 40
[36] Cline D 1986 *Annu. Rev. Nucl. Part. Sci.* **36** 683
[37] Digital Gamma Finder (DGF-4C Revision D) www.xia.com/DGF_products.html
[38] http://mesytec.com/products/nuclear-physics/MADC-32.html
[39] Lutter R and Schaile O 2000 *IEEE Trans. Nucl. Sci.* **47** 280
[40] Essel H and Kurz N http://win.gsi.de/daq
[41] Brun R *et al* http://root.cern.ch
[42] Pakarinen J *et al* 2015 *JPS Conf. Proc.* **6** 020011
[43] Czosnyka T, Cline D and Wu C Y 1983 *Bull. Am. Phys. Soc.* **28** 745
[44] Cline D Gosia User Manual for Simulation and Analysis of Coulomb Excitation Experiments (Rochester, NY, 2012) http://pas.rochester.edu/~cline/Gosia/
[45] http://nndc.bnl.gov/nudat2/
[46] Zielińska M, Gaffney L P, Wrzosek-Lipska K, Clément E, Grahn T, Kesteloot N, Napiorkowski P, Pakarinen J, Van Duppen P and Warr N 2016 *Eur. Phys. J.* A **52** 99
[47] Alster J 1966 *Phys. Rev.* **141** 1138
[48] Ziegler J F and Peterson G A 1968 *Phys. Rev.* **165** 1337
[49] Joye A M R, Baxter A M, Hinds S, Kean D C and Spear R H 1978 *Phys. Lett.* **72B** 307
[50] Ellegaard C, Barnes P D, Flynn E R and Igo G J 1971 *Nucl. Phys.* A **162** 1
[51] Heenen P-H 2012 *private communication*
[52] Hellemans V, De Baerdemacker S and Heyde K 2008 *Phys. Rev.* C **77** 064324
[53] Pakarinen J *et al* 2007 *Phys. Rev.* C **75** 014302
[54] Carlsson G, Toivanen J and Pastore A 2012 *Phys. Rev.* C **86** 014307
[55] Qi C, Jia L Y and Fu G J 2016 *Phys. Rev.* C **94** 014312
[56] Nara Singh B S 2015 HIE-ISOLDE letter of intent *CERN Report* CERN-INTC-2015-047 (https://cds.cern.ch/record/002059390?ln=en)